Applied Catalysis B: Environment and Energy 348 (2024) 123836

Contents lists available at ScienceDirect

Applied Catalysis B: Environment and Energy

journal homepage: www.elsevier.com/locate/apcatb

Solar driven ammonia synthesis with Co-TiO_x and Ag nanowires enhanced Cu_2ZnSnS_4 photocathodes

Shujie Zhou [a,1], Kaiwen Sun [b,1], Cui Ying Toe [a,e,*], Jialiang Huang [b], Ao Wang [b], Jodie Yuwono [a,f], Priyank Kumar [a], Tao Wan [c], Doudou Zhang [d], Zhipeng Ma [a], Jitraporn Vongsvivut [g], Dewei Chu [c], Xiaojing Hao [b,**], Rose Amal [a,**]

[a] School of Chemical Engineering, UNSW Sydney, Sydney, NSW 2052, Australia
[b] School of Photovoltaic and Renewable Energy Engineering, UNSW Sydney, Sydney, NSW 2052, Australia
[c] School of Material Science and Engineering, UNSW Sydney, Sydney, NSW 2052, Australia
[d] School of Engineering, The Australian National University, Canberra, ACT 2601, Australia
[e] School of Engineering, University of Newcastle, Callaghan, NSW 2308, Australia
[f] School of Chemical Engineering, The University of Adelaide, Adelaide, SA 5005, Australia
[g] Infrared Microspectroscopy (IRM) Beamline, ANSTO-Australian Synchrotron, Clayton, VIC 3168, Australia

ARTICLE INFO

Keywords:
Photoelectrochemical ammonia synthesis
Nitrate reduction
Cu_2ZnSnS_4 photocathode
Surface catalytic site engineering

ABSTRACT

Restoring ammonia from waste nitrate stands as a promising strategy for reducing reliance on the energy-intensive Haber-Bosch process and tackling environmental pollutants. Advancing the catalytic aspects of photoelectrochemical (PEC) ammonia synthesis via waste nitrate reduction is of great importance to enhance its viability for sustainable chemical production. However, this process still suffers from low ammonia faradaic efficiency (FE) with high operational potential due to its involvement in multi-electron reactions. Herein, we integrated a cobalt-doped TiO_x (Co-TiO_x) cocatalyst and Ag nanowires (NWs) electron extraction layer onto TiO_x/CdS/Cu_2ZnSnS_4 (CZTS) photocathode, achieving nearly 100 % ammonia FE and an onset potential of ~0.49 V vs. RHE. Evidenced by the in-situ synchrotron-radiated FTIR (SR-FTIR) and theoretical calculations, the increased ratio of surface oxygen vacancy sites (Vo) induced by Co-TiO_x is crucial for the key reaction intermediates adsorption (i.e. *NO_3 and *NO_2) for subsequent ammonia production. Moreover, the transparent Ag NWs facilitates the electron extraction from TiO_x/CdS/CZTS to the surface catalytic sites. Powered by CZTS solar cells, a standalone solar-to-ammonia system has been demonstrated with outstanding activity and catalytic performance.

1. Introduction

In this transformative era of energy technology, there exists a pressing imperative to transition towards sustainable practices and the utilization of renewable energy sources, most notably solar power, in the pursuit of a novel paradigm for chemical manufacturing [1,2]. The historical reliance on fossil fuels, which has underpinned our advances, is no longer tenable in the face of the ever-expanding global population's needs. Consequently, with shifting towards renewable energy solutions, it is of great importance to embrace a circular economy ethos by advancing catalysis technology that repurposes waste and diminishes our reliance on finite resources [3].

Nitrogen-containing fertilizers (i.e. ammonia) in agriculture have been crucial in feeding the growing global population over the past century [4–6]. Nevertheless, the overuse of fertilizers can lead to an excessive accumulation of nitrate in the soil, disrupting the natural nitrogen cycle and posing a severe threat to human and marine life [7,8]. Furthermore, the production of ammonia has traditionally relied on the Haber-Bosch process, which is known for being energy-intensive and responsible for more than 2 % of the world's greenhouse gas emissions [9–11]. In this regard, restoring ammonia from waste nitrate (NO_3^-) provides an environmentally friendly approach to convert contaminants

* Corresponding author at: School of Chemical Engineering, UNSW Sydney, Sydney, NSW 2052, Australia.
** Corresponding authors.
E-mail addresses: CuiYing.Toe@newcastle.edu.au (C.Y. Toe), xj.hao@unsw.edu.au (X. Hao), r.amal@unsw.edu.au (R. Amal).
[1] These authors contributed equally.

https://doi.org/10.1016/j.apcatb.2024.123836
Received 11 December 2023; Received in revised form 2 February 2024; Accepted 9 February 2024
Available online 10 February 2024

NO_3^- into value-added chemicals. Recovering ammonia from contaminants can also contribute to reducing the global carbon footprint, achieving nitrogen cycle enclosure, and promoting a circular economy [12–14]. Moreover, among different processes for nitrate conversion to ammonia, photoelectrochemical (PEC) ammonia synthesis offers even more advantages which enables the direct conversion from solar energy. The first demonstration of PEC ammonia synthesis was date back to 1977 when TiO_2 photocatalyst was found to generate NH_3 by N_2 reduction reaction under ultraviolet light [15]. Since then, a few photocathodes such as Cu_2O, [16] BiOI, [17] black phosphorus,[18] Si ,[19] etc., have been reported for PEC ammonia synthesis from N_2. However, the faradaic efficiency and yield of PEC ammonia synthesis from N_2 reduction are relatively low (less than 40 % faradaic efficiency and tens $\mu g\ cm^{-2}\ h^{-1}$), [20,21] due to the poor solubility of N_2 in aqueous solution and the serious competing reaction of hydrogen evolution reaction (HER). In 2022, Lee et. al demonstrated an ordered silicon nanowire array photocathode with Au as cocatalyst for ammonia synthesis from nitrate reduction, [22] showing the feasibility of PEC nitrate reduction to produce ammonia. Our previous demonstration on PEC ammonia synthesis from nitrate reduction turned out to be a successful attempt to restore ammonia from nitrate-rich wastewater directly driven by renewable solar energy [23]. However, even though the generation of ammonia from nitrate reduction ($NO_3^- + 9H^+ + 8e^- \rightarrow NH_3 + H_2O$) possesses a thermodynamic potential of +0.82 V versus the reversible hydrogen electrode (vs. RHE),[24] a high practically applied potential of −0.3 V vs RHE is commonly applied [25,26]. This negative potential not only increases the possibility of undesired HER, but also results in excess energy consumption [27,28]. Moreover, since the nitrate reduction reaction is a multi-proton coupled electron transfer reaction, various by-products can be produced such as NO_2^-, NO_2, NO, N_2, *etc.,*[29,30] thus limiting the faradaic efficiency (FE) of ammonia as the target product. Therefore, attaining good selectivity under lower applied potentials is still a main challenge for producing ammonia from nitrate reduction to date. Recently, Cu_2ZnSnS_4 (CZTS) materials have emerged as promising photocathodes due to their outstanding light absorption ability, suitable band structure and environmental friendliness [31–33]. Developing a suitable cocatalyst layer for CZTS based photocathodes become increasingly crucial for facilitating the surface reaction kinetics for the ammonia synthesis from nitrate reduction [34]. The cocatalyst materials should be able to accelerate the electron transfer to the surface reaction sites without affecting the light harvesting efficiency of the light absorber [35,36]. Additionally, it is also essential for the designed photocathode to effectively activate reactants NO_3^- and adsorb the related intermediate species for ammonia synthesis while suppressing side reactions (i.e., HER or NO_2^- liberation) [37,38].

Herein, cobalt-doped TiO_x (Co-TiO_x) cocatalyst layer and Ag nanowires (NWs) were successfully loaded on TiO_x/CdS/CZTS photocathode via a facile spin-coating method. Specifically, Ag NWs have shown great potential as the electron extraction layer on top of the TiO_x/CdS/CZTS photocathode, which has been proven to enhance the onset potential of the PEC nitrate reduction reaction by effectively lowering the surface charge resistance. Our theoretical studies also indicate that Co-TiO_x exhibits a lower oxygen vacancy (Vo) forming energy than TiO_x, resulting in an increased number of active Vo. The in-situ synchrotron radiated FT-IR (SR-FTIR) unveils that this cocatalyst design exhibits effective adsorption ability of NO_3^- reactant and key intermediate of $*NO_2$. Additionally, the Vo located near the Ti atom is found to support the $*NO_3$ reactant adsorption and the Vo near the Co atom facilitates the $*NO_2$ protonation process. The obtained Co-TiO_x/Ag/TiO_x/CdS/CZTS photocathode exhibits an onset potential of ~0.49 V vs. RHE, while nearly 100 % ammonia FE has been achieved at −0.1 V vs RHE. Furthermore, a standalone solar to ammonia system (fully powered by CZTS solar cells) has also been established using the obtained photocathode with *ca.* 0.85 % solar to ammonia conversion efficiency, demonstrating the possibility of integrating CZTS solar cells with CZTS based photoelectrodes for solar driven green ammonia production.

2. Experimental section

2.1. Synthesis of TiO_x/CdS/CZTS

CZTS precursors were prepared by co-sputtering Cu/ZnS/SnS on Mo-coated soda-lime glass substrates using a magnetron sputtering system (AJA International). A rapid thermal processor (AS-One 150) in a combined sulfur and SnS atmosphere was used for CZTS sulfurization at 560 °C for 3 min. Afterwards, CdS was coated on CZTS thin films by a chemical bath deposition (CBD) method. 0.03 M $CdSO_4$, 1.5 M thiourea and 1.2 M ammonia were used as precursors and the CBD process was 7.5 min at 75 °C. The as obtained CdS/CZTS was then annealed on a hot plate at 270 °C for 10 min before TiO_x layer deposition. 0.2 M titanium diisopropoxide bis(acetylacetonate) (TIAA) solution in isopropanol is used as the TiO_x precursor, which was aged overnight before use. The TiO_x film was spray coated with an automatic spraying system using N_2 as carrier gas with simultaneous heating applied by a hotplate at 250 °C. The total duration of spray coating process was set for 240 s, with pulsed spray cycle set at 1 s on and 19 s off. After the spray coating process, the heating process was kept for another 10 min after the spray coating process.

2.2. Synthesis of Ag/TiO_x/CdS/CZTS

Ag NWs were prepared according to a polyol process [39,40]. Moreover, Ag/TiO_x/CdS/CZTS photocathodes were prepared using spin-coating method, with 180 μL Ag NWs suspension dropped on the TiO_x/CdS/CZTS followed by 500 rpm for 20 s. 4 cycles were applied for obtaining Ag/TiO_x/CdS/CZTS with good conductivity and transparency.

2.3. Synthesis of Co-TiO_x/Ag/TiO_x/CdS/CZTS

Co-TiO_x layer was prepared by a sol-gel and spin-coating method. Tris(acetylacetonato)cobalt (III) ($Co(Acac)_3$) is used as the cobalt precursor, which was dissolved in 0.2 M TIAA isopropanol solution with an atomic ratio of Co/Ti = 2.5 %, followed by sonication for 30 min to obtain a homogeneous solution. Afterwards, 180 μL Co-TiO_x precursor was dropped on Ag/TiO_x/CdS/CZTS surface followed by spin-coating at 2000 rpm for 20 s. It was then transferred to a hot plate heated at 250 °C for 10 min. This process was repeated for 2 times to prepare Co-TiO_x/Ag/TiO_x/CdS/CZTS photocathode.

The fabrication of CZTS solar cells and the material characterizations are available in Supplementary information.

3. Results and discussion

3.1. Characterisations of photocathodes

Fig. 1a illustrates the schematic diagram of Co-TiO_x/Ag/TiO_x/CdS/CZTS preparation based on the method described in the experimental section supporting information First, TiO_x was spray coated on CdS/CZTS at 250 °C to attain good photogenerated charge transfer performance and a desired amount of Ti^{3+}/oxygen vacancy as active sites, as discussed in our previous work [23]. Uniform TiO_x layer deposited on CdS/CZTS was obtained, as illustrated in Fig. 1b. Subsequently, Ag NWs were deposited on TiO_x/CdS/CZTS via a facile spin-coating method. The deposited Ag NWs were around 60 nm in diameter and more than 50 μm in length (Fig. S3a-b), which were homogeneously distributed on TiO_x/CdS/CZTS (Fig. 1c). This was followed by spin coating of 2.5 % Co-doped TiO_x (Co-TiO_x) on the Ag/TiO_x/CdS/CZTS. $Co(Acac)_3$ was used as the Co precursor in TIAA with the precursor concentrated adjusted to produce 2.5 % Co doping with respect to Ti. The uniform overlayer of Co-TiO_x can be clearly observed on top of Ag/TiO_x/CdS/CZTS (Fig. 1d), indicating the successful fabrication of Co-TiO_x/Ag/TiO_x/CdS/CZTS.

The thickness of Co-TiO_x/Ag/TiO_x/CdS/CZTS was analysed from the

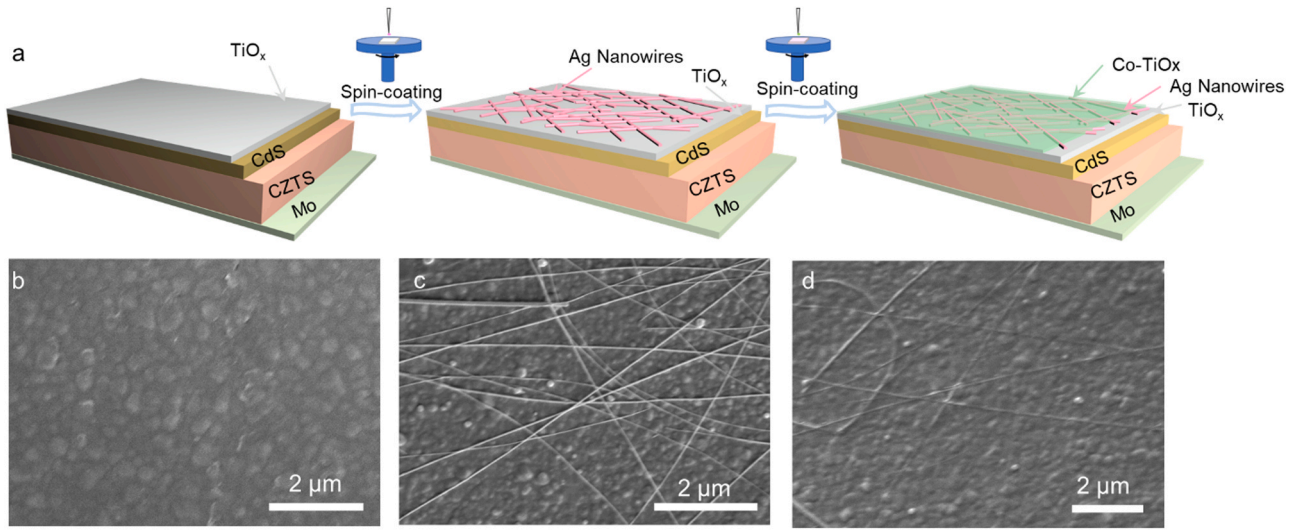

Fig. 1. a) Schematic diagram of preparing Co-TiO_x/Ag/TiO_x/CdS/CZTS; corresponding SEM images of b) TiO_x/CdS/CZTS, c) Ag/TiO_x/CdS/CZTS, d) Co-TiO_x/Ag/TiO_x/CdS/CZTS.

cross-sectional SEM image (Fig. S4), where the total thickness of the photocathode is 800 nm with approximately 650 nm CZTS, 80 nm CdS and 50 nm Co-TiO_x/Ag/TiO_x layer. Additionally, the formation of Co-TiO_x and Ag NWs was confirmed by scanning transmission electron microscopy (STEM) with energy-dispersive X-ray spectroscopy (EDS) mapping. It is evident that TiO_x exhibits uniform distribution on CdS

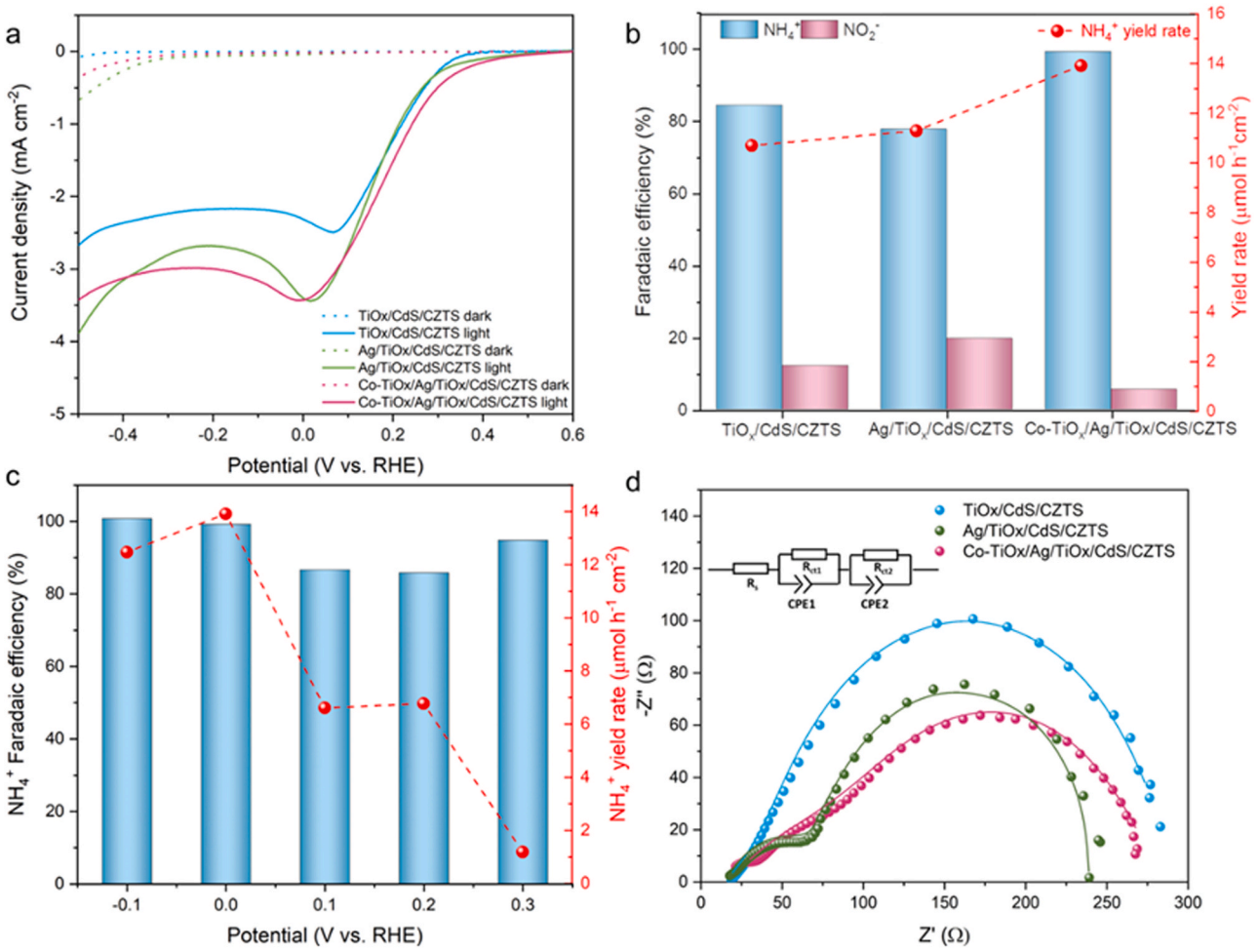

Fig. 2. a) LSV curves of TiO_x/CdS/CZTS, Ag/TiO_x/CdS/CZTS and Co-TiO_x/Ag/TiO_x/CdS/CZTS photocathodes; b) corresponding FE of different products and NH_4^+ yield rate at 0 V vs. RHE; c) NH_4^+ FE and yield rate of Co-TiO_x/Ag/TiO_x/CdS/CZTS photocathodes at different potentials; d) EIS Nyquist plot of different photocathodes at 0 V vs RHE under illumination, inset is the corresponding equivalent circuit. The electrolyte is 0.1 M KNO_3 and 10 mM H_2SO_4 (pH=1.8).

while Co exists on top of the TiO_x layer (Fig. S5). Moreover, the Ag NWs are also seen on top of TiO_x, which is consistent with the SEM images in Fig. 1. The atomic ratio of Co in TiO_x is evidenced by the STEM-EDS line scans of atomic fractions as shown in Fig. S6. It can be observed that around 2.1 % of cobalt is detected together with Ag on top of TiO_x, indicating the formation of thin layer Co-TiO_x on top of Ag.

In addition to the morphology and composition structure analysis of Co-TiO_x and Ag on TiO_x/CdS/CZTS, it is important to consider the possible light blocking effect of the additional layers. Therefore, UV–vis transmittance of Ag NWs and Co-TiO_x/Ag NWs on TiO_x/FTO substrates has been tested. Ag NWs with 2, 4 and 6 spin-coating cycles on TiO_x/FTO have been prepared, which are denoted as Ag2/TiO_x/FTO, Ag4/TiO_x/FTO and Ag6/TiO_x/FTO, respectively. It is observed that the transmittance of Ag/TiO_x does not exhibit an obvious decrease compared to TiO_x/FTO (Fig. S7a), indicating good transparency of the Ag NWs. With the increased spin-coating cycles, the transmittance of Ag6/TiO_x FTO is slightly lower than that of other samples, which might result from the excessive coating of Ag. Therefore, 4 cycles of Ag coating is selected as the optimal Ag loading to attain both improved charge extraction and satisfactory transmittance. For Co-TiO_x coating, the overall transmittance of Co-TiO_x/Ag/TiO_x exhibits a minimal decrease in the region of 400–800 nm, as is shown in Fig. S7b. This indicates that there is a negligible light blocking effect after the deposition of Co-TiO_x/Ag on TiO_x/CdS/CZTS. In addition, a different ratio of Co doping has been prepared on TiO_x/CdS/CZTS (Fig. S8) and 2.5 % is seen to be the optimal ratio, which demonstrates the best onset potential.

3.2. PEC nitrate reduction performance evaluation

The as-obtained TiO_x/CdS/CZTS, Ag/TiO_x/CdS/CZTS and Co-TiO_x/Ag/TiO_x/CdS/CZTS photocathodes were evaluated for their PEC nitrate reduction performance. The linear sweep voltammetry (LSV) curves in Fig. 2a show that all three samples exhibited obvious photocurrent current upon illumination. In addition, for TiO_x/CdS/CZTS, it exhibits an onset potential of ~0.36 V vs. RHE (defined at where cathodic photocurrent density reaches 50 μA/cm^2), [41]. which is consistent with our previous work [23]. After Ag NWs coating, a positive shift of the onset potential is observed, reaching ~0.45 V vs. RHE. Photocurrent density of Ag/TiO_x/CdS/CZTS is also increased when compared to TiO_x/CdS/CZTS, resulting from the improved electron extraction performance by Ag coating. Upon Co-TiO_x coating, the onset potential is further shifted to 0.49 V vs. RHE. The improved onset potential as well as increased current density are observed after Ag NWs and Co-TiO_x coating, suggesting a more efficient reaction activity.

All three photocathodes exhibit different FE towards NH_4^+ at 0 V vs. RHE, as shown in Fig. 2b. The possible gas products have been also tested via gas chromatography (GC) after the reaction and no gas product such as H_2 or N_2 has been detected for all the samples. It is seen that the TiO_x/CdS/CZTS exhibits a FE of 84.4 % towards NH_4^+, which is consistent with our previous result in applying TiO_x as the cocatalyst on CdS/CZTS. However, upon additional coating of Ag NWs, the FE towards NH_4^+ is reduced to 77.8 % with the NO_2^- FE increased to 19.7 %. Moreover, it is seen that the NH_4^+ yield rate of Ag/TiO_x/CdS/CZTS (11.30 μmol/h cm^2) is slightly higher than that of TiO_x/CdS/CZTS (10.70 μmol h^{-1} cm^{-2}) resulting from the increased photocurrent density with the coating of Ag NWs. This suggests that despite enhancing the overall activity towards nitrate reduction (as illustrated by the improved current density and onset potential), the presence of Ag NWs results in more NO_2^- liberation instead of improving the target ammonia production. Interestingly, with the additional layer of Co-TiO_x on Ag/TiO_x/CdS/CZTS, the FE towards NH_4^+ reaches up to 99.2 % with a significant decrease of NO_2^- FE at 0 V vs. RHE, indicating that Co-TiO_x exhibits a more favourable selectivity towards ammonia while suppressing the NO_2^- generation. In addition to the enhanced NH_4^+ FE, the yield rate of NH_4^+ reaches up to 13.91 μmol h^{-1} cm^{-2} at 0 V vs. RHE, which is 1.3 times of TiO_x/CdS/CZTS, benefitting from both the enhanced reaction activity and ammonia selectivity.

The NH_4^+ FE and yield rate of Co-TiO_x/Ag/TiO_x/CdS/CZTS at different applied potentials are shown in Fig. 2c, where it exhibits excellent ammonia FE beyond 85 % among all the tested potentials. Nearly 100 % FE of ammonia is achieved at −0.1 V vs. RHE and the highest yield rate of 13.91 μmol h^{-1} cm^{-2} with 99.2 % FE is achieved at 0 V vs RHE. To further confirm the origin of ammonia, isotope labelling experiments using $K^{14}NO_3$ and $K^{15}NO_3$ as reactant for Co-TiO_x/Ag/TiO_x/CdS/CZTS at 0 V vs. RHE have been conducted. It can be seen from Fig. S9 that when using $K^{14}NO_3$ as reactant, triple peaks of $^{14}NH_4^+$ are observed. In contrast, double peaks of $^{15}NH_4^+$ are observed for when $^{15}NO_3^-$ is employed during the PEC reduction process. These results verified that the formation of ammonia is indeed originates from the nitrate-N. Electrochemical impedance spectroscopy (EIS) was tested to study the charge transfer resistance and the surface resistance after Ag NWs coating and Co-TiO_x coating. It is seen in Fig. 2d that two semicircles are observed, where the first semicircle at high frequency is related to charge transfer resistance (R_{ct1}) within the photocathode and the second semicircle at low frequency accounts for the surface resistance (R_{ct2}) at the photocathode/electrolyte interface, respectively [42, 43]. As shown in the inset of Fig. 2d and the fitting results in Table S1, all the samples show similar R_s, which accounts for the sheet resistance of the system. Interestingly, after Ag NWs coating, the R_{ct2} significantly reduces to 147.1 Ω, compared to 204.7 Ω of TiO_x/CdS/CZTS. This indicates that the Ag NWs coating facilitates the electron transfer and injection from TiO_x/CdS/CZTS to the electrolyte, which is consistent with the improvement of the photocurrent observed in Fig. 2a. Moreover, after another coating of Co-TiO_x, R_{ct1} slightly increases compared to TiO_x/CdS/CZTS and Ag/TiO_x/CdS/CZTS, which might be caused by the additional heating process required for Co-TiO_x coating. However, the R_{ct2} is reduced to 126.8 Ω after Co-TiO_x coating, indicating a decreased charge transfer resistance at the photocathode/electrolyte interface, which is associated with the enhanced nitrate reduction activity evidenced in Fig. 2. Incident photon-to-electron conversion efficiency (IPCE) of the obtained photocathodes were provided in Fig. S10, which also indicates the Co-TiO_x/Ag/TiO_x/CdS/CZTS exhibits enhanced charge separation performance with the deposition of Ag. Based on the above, the optimized onset potential, increased ammonia yield and improved NH_4^+ FE are successfully obtained by applying Co-TiO_x cocatalyst layer and Ag NWs electron extraction interlayer on TiO_x/CdS/CZTS. Moreover, the band alignment of the Co-TiO_x/-Ag/TiO_x/CdS/CZTS was shown in Fig. S12, where the photogenerated electrons from CZTS are moved from the conduction band of CZTS to that of CdS, and finally accumulated and consumed at the Co-TiO_x reaction surface.

3.3. Investigation of the catalytic mechanism

Inspired by the greatly improved reaction activity and NH_4^+ selectivity, further investigation has been focused on understanding the role of Ag NWs and Co-TiO_x coating in enhancing the performance. In this regard, X-ray photoelectron spectroscopy (XPS) was carried out to probe the surface chemical states. As indicated from the Ti 2p spectra in Fig. S13, two peaks at Ti $2p_{3/2}$ 458.8 and Ti $2p_{1/2}$ 464.5 eV are observed for TiO_x and the peak width between Ti $2p_{3/2}$ and Ti $2p_{1/2}$ is approximate 5.7 eV, indicating the existence of Ti^{4+} oxidation state in stoichiometric TiO_2 [44]. This indicates that the prepared TiO_x and Co-TiO_x are dominant by Ti^{4+} while they also contain Ti^{3+} due to the formation of oxygen vacancy, which will be discussed in the following part. Interestingly, after Ag NWs coating, the Ti 2p peaks show an obvious positive shift to 459.5 and 465.1 eV. The positive shift in binding energy indicates a reduced electron density around Ti after Ag NW coating, [45] which is caused by electron extraction from TiO_x, suggesting an improved electron collection ability [46,47]. Moreover, when another Co-TiO_x layer is coated, the Ti 2p peaks shift back to 464.5 and 458.8 eV, which indicates the redistribution of electrons collected by Ag NWs to

the Co-TiO_x layer. From the Ti 2p spectra, it is revealed that the Ag NWs mainly work as the electron extraction layer in the Co-TiO_x/-Ag/TiO_x/CdS/CZTS photocathode, which contributes to better electron transfer from TiO_x/CdS/CZTS to Co-TiO_x.

Furthermore, in order to understand the role of Co-TiO_x in improving the ammonia FE, the XPS results of Ti 2p and O 1s spectra of TiO_x and Co-TiO_x are compared in Fig. 3. As observed from Fi 3a-b, both TiO_x and Co-TiO_x exhibit a dominant peak centred at 458.8 eV, which corresponds to Ti^{4+}, suggesting the formation of stoichiometric TiO_2[48]. It is evidenced that a small characteristic peak at lower binding energy (457.6 eV) is corresponded to Ti^{3+}, which indicates the existence of unpaired Ti^{3+} with Vo[49,50]. It is found that by integrating the peak area, Co-TiO_x has higher ratio of Ti^{3+} (as calculated by the peak area of $Ti^{3+}/(Ti^{3+}+Ti^{4+})$=7.13 %) compared to TiO_x (6.28 %). This is also verified by the O 1s spectra, where the peak located at 530.3 eV is originated from the lattice oxygen of Ti-O bond [51]. In addition, as indicated by the peak at binding energy of 531.9 eV in Fig. 3c-d, the formation of Vo within both Co-TiO_x and TiO_x is also verified [52,53]. Likewise, Co-TiO_x exhibits a higher amount of Vo compared to TiO_x, as indicated by the larger peak ratio of Vo. In addition to the increased amount of Vo originating from the Co doping, it is indicated from the Co 2p spectra in Fig. S14 that the Co in Co-TiO_x exists as Co^{2+} states with Co $2p_{3/2}$ and Co $2p_{1/2}$ peaks at 780.8 and 796.7 eV, respectively. The satellite features at approximately 786.0 and 802.7 eV is well aligned to Co^{2+} [54]. In this regard, it is deduced that Co dopant in TiO_x exhibits as Co^{2+} in TiO_2 matrix, which results in a more distorted structure and thus increased Vo sites. Based on these results, it is revealed that Ag NWs contribute to enhanced electron extraction from TiO_x/CdS/CZTS, while Co-TiO_x is the cocatalyst that contains Vo as the surface active sites, improving the overall ammonia FE.

In order to gain a better understanding of the mechanism of PEC ammonia production from nitrate reduction on Co-TiO_x/Ag/TiO_x/CdS/CZTS, in-situ SR-FTIR was conducted. As demonstrated in Fig. 4a and Fig. S15, the in-situ SR-FTIR set-up consists of a synchrotron-radiated IR beam with reflection mode, a potentiostat to apply external bias and record the current and a customised in-situ reactor with an optic-fibre for illumination. Chrono-amperometry method of 300 s was applied from open circuit potential to −0.3 V vs. RHE with the step of 0.1 V to test the performance at each potential. The negative peak located at 1040 cm^{-1} is related to the adsorption of free nitrate from the electrolyte, which is gradually reducing due to the consumption of NO_3^- (Fig. 4b-c).[55] In addition, the positive broad peak around 2010 cm^{-1} (Fig. S16) is related to the bridging nitrate, [56] where the N-O bond from nitrate occupies oxygen vacancy sites of Co-TiO_x. The appearance of bridging nitrate at a very positive potential of 0.3 V vs RHE indicates that the Co-TiO_x/Ag/TiO_x/CdS/CZTS exhibits a good reactant adsorption ability. The negative band at 1040 cm^{-1} is getting more obvious with increased applied potential, indicating the progression of the nitrate reduction reaction. SR-FTIR results of TiO_x/CdS/CZTS are shown in Fig. S17, which suggests a much weaker signal of nitrate consumption

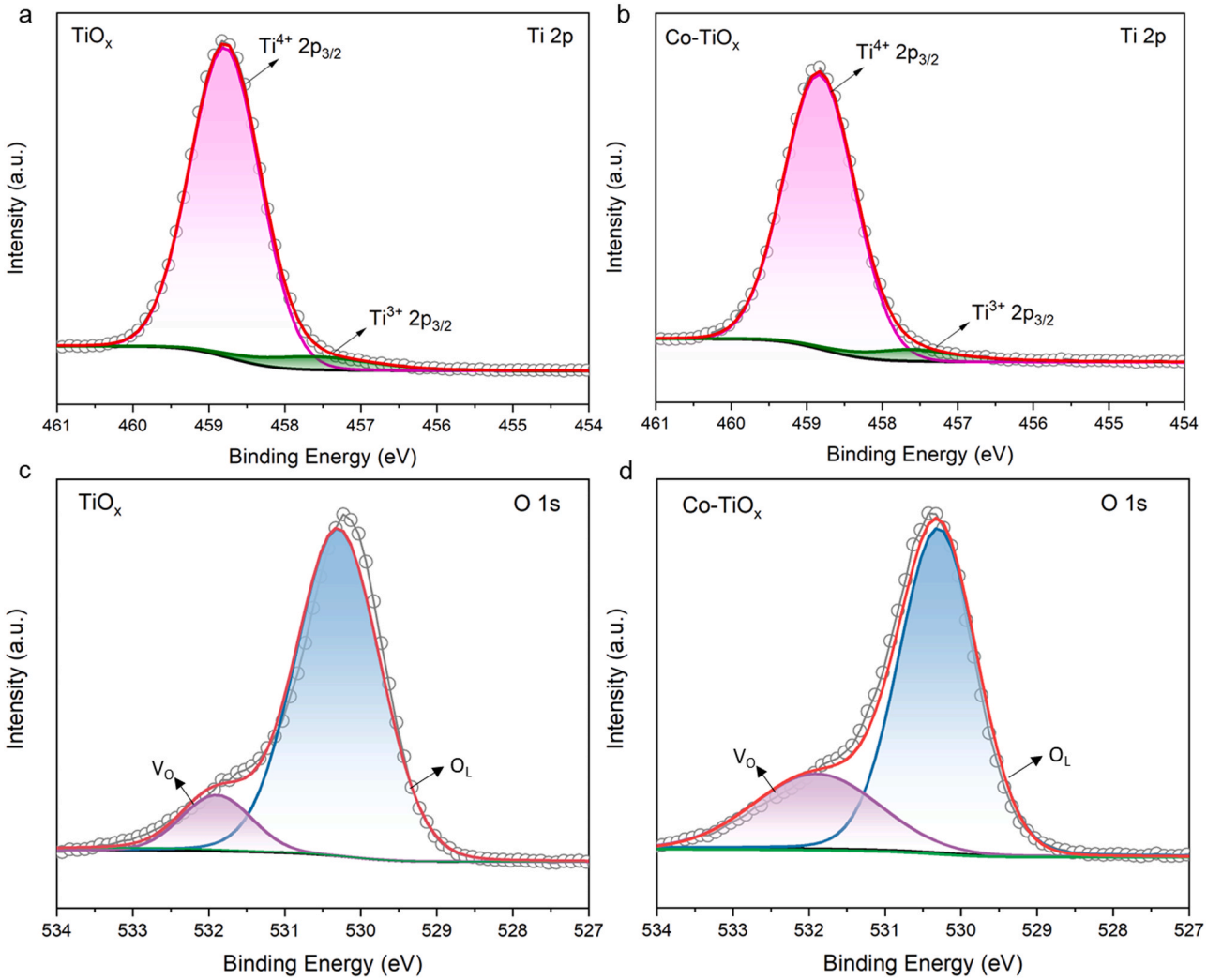

Fig. 3. a-b) Ti 2p spectra of TiO_x and Co-TiO_x; c-d) O 1 s spectra of TiO_x and Co-TiO_x.

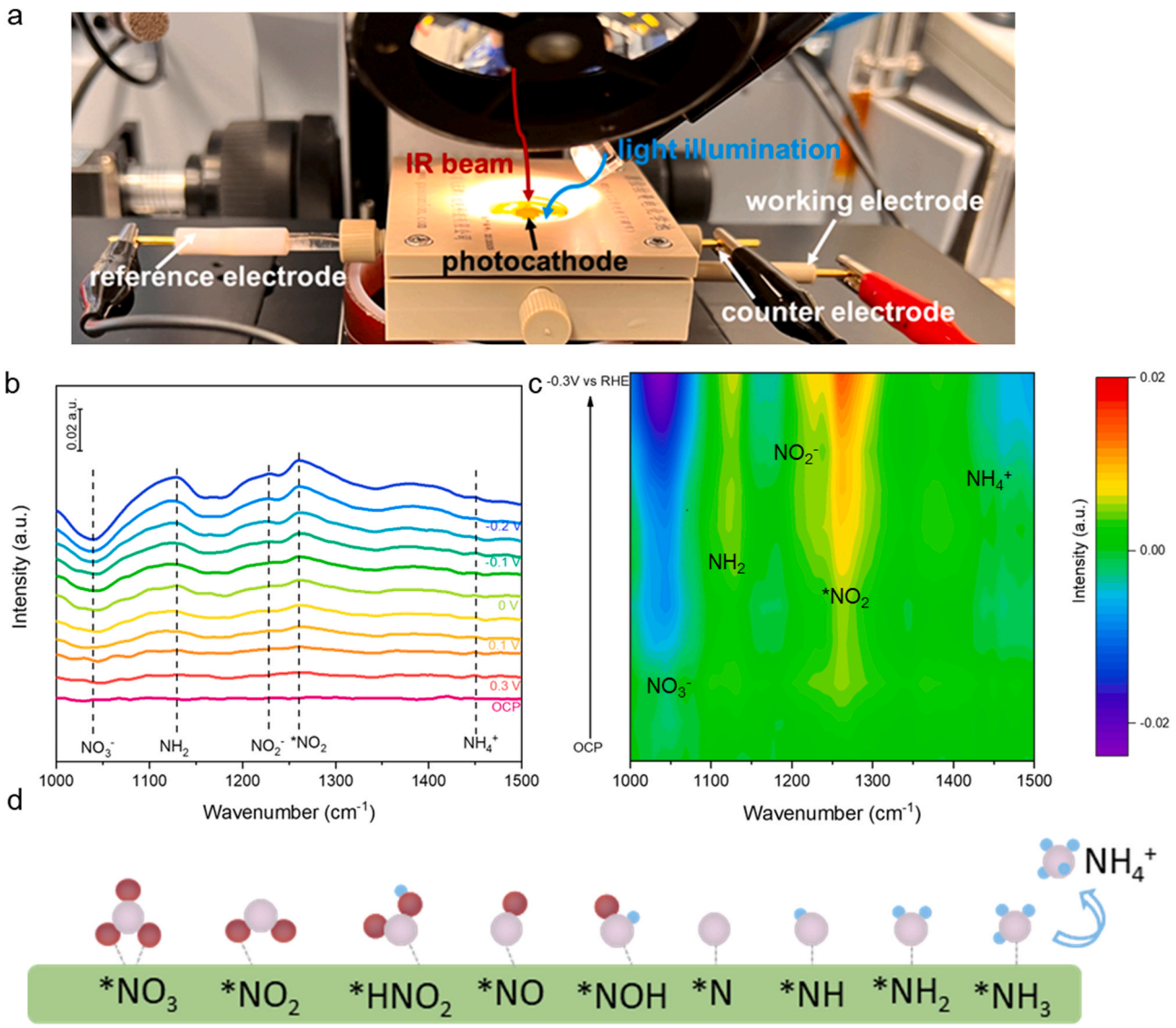

Fig. 4. a) Photo of the in-situ SR-FTIR set-up; b) the in-situ SR-FTIR spectra (in the wavenumber from 1000 to 1500 cm^{-1}) of Co-TiO_x/Ag/TiO_x/CdS/CZTS for PEC nitrate reduction with different applied potentials from open circuit potential to −0.3 V vs. RHE and c) the corresponding contour image, d) proposed reaction pathway from nitrate to ammonia.

peak of 1040 cm^{-1} found at higher potential. This indicates TiO_x/CdS/CZTS exhibits relatively poor adsorption ability of $*NO_2$, thereby resulting in lower ammonia FE and yield. Along with the consumption of nitrate, the peaks located at 1237 and 1260 cm^{-1} are observed as positive bands, which are related to the formation of NO_2^- and $*NO_2$ intermediates [57]. This indicates that nitrate reduction to ammonia is accompanied by the formation of nitrites as stable intermediates. Moreover, the positive band located at ~1130 cm^{-1} is assigned to the formation of $*NH_2$, which increases with the applied potential, suggesting the adsorption and accumulation of $*NH_2$ on the surface [58]. Similarly, a small peak at 1450 cm^{-1} corresponding to the formation of NH_4^+ is witnessed with the increase of applied potential, [59] suggesting the generation of ammonia. In addition, a broad band around 2900–3200 cm^{-1} associated with ammonia is also evidenced (Fig. S16) in Co-TiO_x/Ag/TiO_x/CdS/CZTS. The in-situ SR-FTIR results unveil the reaction pathway from NO_3^- to NH_4^+ as illustrated in Fig. 4d, during which the NO_3^- is firstly adsorbed and reduced to NO_2^- with $*NO_2$ adsorbed and gradually deoxygenated and pronated to produce NH_4^+. In addition, from the contour image in Fig. 4c, it shows the adsorption and consumption of NO_3^- with simultaneous adsorption of $*NO_2$, which is considered as a key step for generating ammonia as the product. Furthermore, the in-situ SR-FTIR spectra of Co-TiO_x/-Ag/TiO_x/CdS/CZTS under dark condition is provided as Fig. S18. No obvious peak changes have been witnessed with increasing the applied potential from open circuit potential to −0.3 V vs RHE, which indicates no reaction occurs due to the low dark current as shown in Fig. 2a. Based on the SR-FTIR results, the reaction pathway of nitrate reduction to ammonia on Co-TiO_x/Ag/TiO_x/CdS/CZTS has been proposed as Fig. 4d [60].

In order to gain deeper understanding of the formation of oxygen vacancy and the enhancement mechanism of the ammonia FE, density functional theory (DFT) calculation has been conducted. Fig. 5a–d illustrate the model of pristine structure of TiO_2, Co-doped TiO_2, TiO_2 with 1 Vo and Co-doped TiO_2 with 1 Vo, respectively. As evidenced by Fig. 5e, Co^{2+} doping into TiO_2 greatly reduces the oxygen vacancy formation energy, from 4.27 eV of pristine TiO_2 to 0.66 eV of Co-TiO_2. This indicates the introduction of Co dopant facilitates the formation of Vo, thus resulting in more Vo, as observed from Co-TiO_x XPS results. In this regard, two different Vo have been created in the Co-TiO_x model, which is denoted as Ti-Vo and Co-Vo, respectively. As is illustrated in Fig. 5f, the adsorption energy of $*NO_3$ reactant is firstly studied. Interestingly, it is found that for both 1 Vo and 2 Vo, Ti-Vo exhibits obviously lower

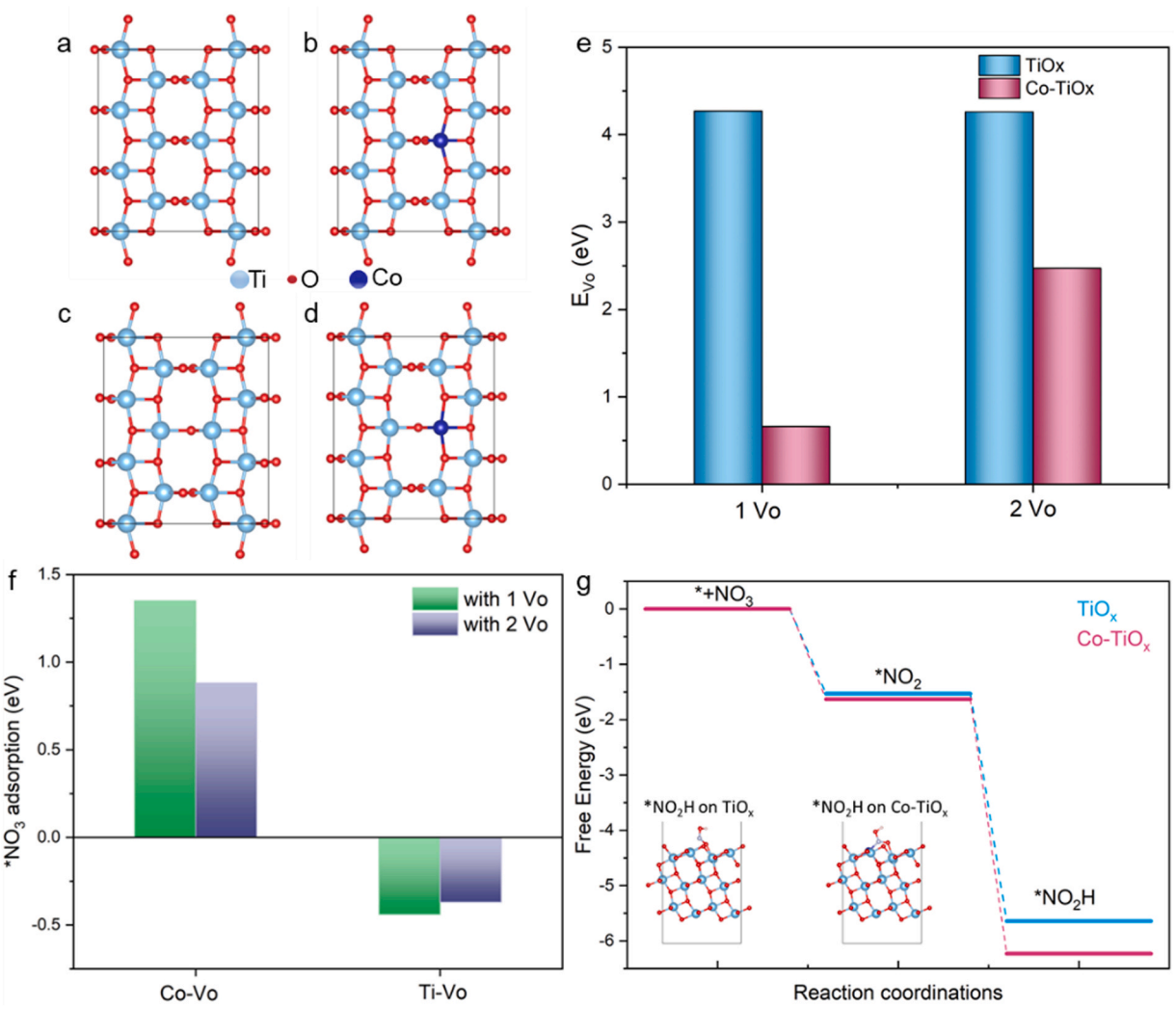

Fig. 5. Slab models of a) pristine structure of TiO_2 and b) Co-TiO_2; c) TiO_2 with 1 Vo and d) Co-TiO_2 with 1 Vo; e) Vo formation energy of TiO_2 and Co-TiO_2; f) *NO_3 adsorption energy of TiO_2 and Co-TiO_2 with 1 and 2 Vo; g) calculated free energy changes of nitrate reduction reaction on TiO_2 (101) surface and Co-TiO_2 with 1 Vo, inset is the model of *NO_2H adsorbed on different surfaces.

*NO_3 adsorption energy than Co-Vo, indicating that the Vo near Ti is more favourable for *NO_3 adsorption. However, as evidenced by the free energy changes of nitrate reduction on TiO_2 (101) surface and Co-TiO_2 with 1 Vo in Fig. 5g, Co-TiO_2 exhibits more favourable *NO_2 formation energy, indicating that it facilitates the *NO_2 formation compared to Ti-Vo. More importantly, based on the in-situ SR-FTIR results, the*NO_2 adsorption and protonation process is considered as the product-determinate step for nitrate reduction reaction [61]. It is found that the Co-TiO_x shows greatly improved free energy of *NO_2 protonation process to form *NO_2H, which thereby promotes the ammonia pathway instead of generating nitrite. The oxygen vacancy near Co atom (Co-Vo) exhibits not only more favourable *NO_2 forming energy but also better *NO_2 protonation ability, which plays an important role in the ammonia production pathway from nitrate reduction. In addition, Vo near Ti atoms in Co-TiO_x shows better *NO_3 adsorption ability, enabling a better nitrate reduction activity of Co-TiO_x. Working synergistically, Co-TiO_x enables effectively and selectively generating ammonia from nitrate reduction as evidenced by the improved PEC performance illustrated in Fig. 2.

3.4. Demonstration of solar driven ammonia synthesis system

It is summarised in Table S2 that the demonstrated Co-TiO_x/Ag/TiO_x/CdS/CZTS photocathode exhibits the best NH_4^+ FE and yield rate among the recent published works. Inspired by the good ammonia selectivity obtained of Co-TiO_x/Ag/TiO_x/CdS/CZTS, a standalone solar to ammonia system was constructed to demonstrate the feasibility of the device. A series connected CZTS based solar cells (PV) has been used to power the system, with Co-TiO_x/Ag/TiO_x/CdS/CZTS working as the photocathode and commercial Ir/RuO_x on Ti mesh as the anode, the schematic of the PV-PEC system is shown as Fig. 6a. The solar to ammonia efficiency (STA) can be calculated via the following equation:

$$\mathrm{STA} = \frac{J_{op} \times A_{electrode} \times E^0}{P_{in} \times A_{solarcell}} \times 100\% \quad (1)$$

where J_{op} is the device operational current density (mA/cm^2), $A_{electrode}$ is the electrode area (0.5 cm^2), E^0 is the equilibrium potential of the overall reaction (E^0=1.23–0.82 =0.41), where NO_3^- to NH_4^+ reaction ($NO_3^- + 9\,H^+ + 8\,e^- \rightarrow NH_3 + 3\,H_2O$, E=0.82 V vs RHE) happens at the cathode compartment, [24] and the oxygen evolution reaction ($2\,H_2O + 4\,h^+ \rightarrow O_2 + 4\,H^+$, E=1.23 V vs. RHE) happens at the anode compartment [62]. P_{in} is the power input of the device, which is illuminated using a solar simulator to generate AM 1.5 G (100 mW/cm^2) and $A_{solarcell}$ is the area of solar cell (0.448 cm^2). As indicated in the intersection of I-V curve of CZTS solar cells (PV) and the LSV curve of 2-electrode PEC (Fig. 6b), the operational point is found to be 0.93 mA and

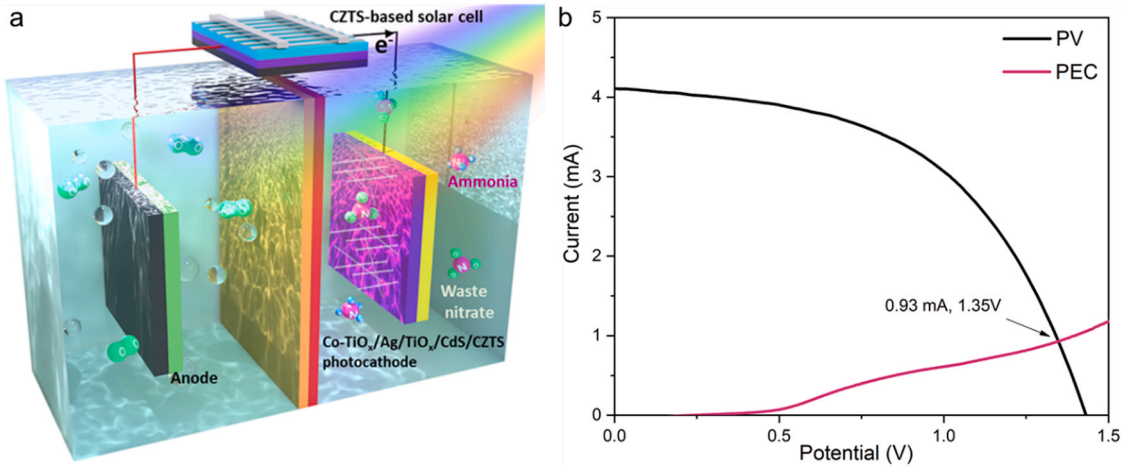

Fig. 6. a) Schematic of the standalone solar to ammonia system based on CZTS based photocathode and a dimensionally stable anode (DSA, Ir- and Ru-coated Ti mesh), powered by a CZTS based solar cell; b) Intersection of I-V curve of CZTS solar cells with the PEC device using Co-TiO_x/Ag/TiO_x/CdS/CZTS as photocathode and DSA.

1.35 V, which accounts for a STA of 0.85 %, demonstrating the potential for establishing a standalone solar to ammonia production system. It should be mentioned that the current PV-PEC system is not the most energy efficient due to the coupling loss when combining the CZTS based solar cell with the PEC system. The operating PV cell is far away from its maximum power point (MPP). There is still room for improvement of the operational condition of the PV-PEC system by power management to minimize the coupling loss [63].

4. Conclusion

In summary, this study presents a novel approach of PEC nitrate reduction for ammonia synthesis by integrating Co-TiO_x and Ag NWs as cocatalyst and electron extraction layers onto TiO_x/CdS/CZTS photocathodes. The obtained Co-TiO_x/Ag/TiO_x/CdS/CZTS demonstrates high performance in terms of both ammonia selectivity and activity, achieving nearly ~100 % FE towards NH_4^+ at −0.1 V vs. RHE with a promising yield rate of 13.91 μmol h^{-1} cm^{-2} at 0 V vs. RHE. It is found that by using Ag NWs as an electron extraction layer, significantly reduced charge transfer resistance from TiO_x/CdS/CZTS is obtained, contributing to increased reaction activity with improved onset potential and photocurrent density. The catalytic mechanism of PEC nitrate reduction has also been comprehensively studied. The incorporation of Co-TiO_x as a cocatalyst layer introduces a significant number of Vo active sites due to Co^{2+} dopant. These Vo sites play a pivotal role in facilitating the adsorption of crucial reaction intermediates, such as $*NO_3$ and $*NO_2$ for ammonia production. Additionally, the Vo located near the Ti atom supports the $*NO_3$ reactant adsorption and the Vo near the Co atom facilitates the $*NO_2$ protonation process, as indicated by DFT results. In-situ SR FTIR also provides insights into the nitrate reduction pathways, demonstrating that the adsorption and protonation of the key intermediate, $*NO_2$, is the product-determinate step. Powered by CZTS solar cells, a standalone CZTS based solar to ammonia system was developed, delivering a ~0.85 % STA.

CRediT authorship contribution statement

Jodie Yuwono: Writing – original draft, Formal analysis, Data curation. **Priyank Kumar:** Software, Formal analysis, Data curation. **Tao Wan:** Methodology, Investigation, Data curation. **Doudou Zhang:** Writing – original draft, Data curation, Conceptualization. **Zhipeng Ma:** Writing – original draft, Data curation. **Rose Amal:** Writing – review & editing, Supervision, Resources, Project administration, Funding acquisition. **Jitraporn Vongsvivut:** Visualization, Validation, Software, Data curation. **Dewei Chu:** Methodology, Investigation. **Shujie Zhou:** Writing – review & editing, Writing – original draft, Validation, Methodology, Investigation, Formal analysis, Data curation, Conceptualization. **Xiaojing Hao:** Writing – review & editing, Validation, Supervision, Resources, Project administration, Investigation, Funding acquisition, Formal analysis, Conceptualization. **Kaiwen Sun:** Writing – review & editing, Writing – original draft, Validation, Investigation, Data curation, Conceptualization. **Cui Ying Toe:** Writing – review & editing, Writing – original draft, Supervision, Project administration, Data curation, Conceptualization. **Jialiang Huang:** Writing – review & editing, Writing – original draft, Investigation, Formal analysis, Data curation. **Ao Wang:** Validation, Methodology, Investigation, Data curation.

Declaration of Competing Interest

The authors declare that they have no known competing financial interests or personal relationships that could have appeared to influence the work reported in this paper.

Data availability

Data will be made available on request.

Acknowledgements

The authors acknowledge the facilities and the scientific and technical assistance of Microscopy Australia at the Electron Microscope Unit (EMU) and other characterization facilitates within the Mark Wainwright Analytical Centre (MWAC) at UNSW Sydney. The work was supported by the Australian Research Council (ARC) Training Centre for the Global Hydrogen Economy (IC200100023). The authors acknowledge the ARC Discovery Project (ARC DP200102121). X.H. acknowledges the ARC Future Fellowship Programme (FT190100756). K.S. acknowledges the Australian Centre for Advanced Photovoltaics (ACAP) postdoctoral fellowship programme (RG172864-B) and ARC Discovery Early Career Researcher Award (DE230100021). The authors acknowledge the grant (AS2023–1/IRM/19466) for synchrotron IR beamtime at the Australian Synchrotron.

Appendix A. Supporting information

Supplementary data associated with this article can be found in the online version at doi:10.1016/j.apcatb.2024.123836.

References

[1] S.-F. Ng, J.J. Foo, W.-J. Ong, Solar-powered chemistry: Engineering low-dimensional carbon nitride-based nanostructures for selective CO_2 conversion to C_1.C_2 products, InfoMat 4 (1) (2022) e12279, https://doi.org/10.1002/inf2.12279.

[2] N.S. Lewis, D.G. Nocera, Powering the planet: Chemical challenges in solar energy utilization, Proc. Natl. Acad. Sci. USA 103 (43) (2006) 15729–15735, https://doi.org/10.1073/pnas.0603395103.

[3] W.R. Stahel, The circular economy, Nature 531 (7595) (2016) 435–438, https://doi.org/10.1038/531435a.

[4] J.N. Galloway, A.R. Townsend, J.W. Erisman, M. Bekunda, Z. Cai, J.R. Freney, L. A. Martinelli, S.P. Seitzinger, M.A. Sutton, Transformation of the nitrogen cycle: recent trends, questions, and potential solutions, Science 320 (5878) (2008) 889–892, https://doi.org/10.1126/science.1136674.

[5] X. Zhao, K. Zhao, X. Quan, S. Chen, H. Yu, Z. Zhang, J. Niu, S. Zhang, Efficient electrochemical nitrate removal on Cu and nitrogen doped carbon, Chem. Eng. J. 415 (2021) 128958, https://doi.org/10.1016/j.cej.2021.128958.

[6] X. Fu, J. Zhang, Y. Kang, Recent advances and challenges of electrochemical ammonia synthesis, Chem. Catal. 2 (10) (2022) 2590–2613, https://doi.org/10.1016/j.checat.2022.09.001.

[7] J. Lim, C.A. Fernández, S.W. Lee, M.C. Hatzell, Ammonia and nitric acid demands for fertilizer use in 2050, ACS Energy Lett. 6 (10) (2021) 3676–3685, https://doi.org/10.1021/acsenergylett.1c01614.

[8] W. Lin, E. Zhou, J.-F. Xie, J. Lin, Y. Wang, A high power density Zn-nitrate electrochemical cell based on theoretically screened catalysts, Adv. Funct. Mater. 32 (46) (2022) 2209464, https://doi.org/10.1002/adfm.202209464.

[9] C. Smith, A.K. Hill, L. Torrente-Murciano, Current and future role of Haber–Bosch ammonia in a carbon-free energy landscape, Energy Environ. Sci. 13 (2) (2020) 331–344, https://doi.org/10.1039/C9EE02873K.

[10] C.J.M. van der Ham, M.T.M. Koper, D.G.H. Hetterscheid, Challenges in reduction of dinitrogen by proton and electron transfer, Chem. Soc. Rev. 43 (15) (2014) 5183–5191, https://doi.org/10.1039/C4CS00085D.

[11] J.W. Erisman, M.A. Sutton, J. Galloway, Z. Klimont, W. Winiwarter, How a century of ammonia synthesis changed the world, Nat. Geosci. 1 (10) (2008) 636–639, https://doi.org/10.1038/ngeo325.

[12] Y. Xue, Q. Yu, Q. Ma, Y. Chen, C. Zhang, W. Teng, J. Fan, W.-x Zhang, Electrocatalytic hydrogenation boosts reduction of nitrate to ammonia over single-atom Cu with Cu(I)-N_3C_1 Sites, Environ. Sci. Technol. 56 (20) (2022) 14797–14807, https://doi.org/10.1021/acs.est.2c04456.

[13] P.H. van Langevelde, I. Katsounaros, M.T.M. Koper, Electrocatalytic nitrate reduction for sustainable ammonia production, Joule 5 (2) (2021) 290–294, https://doi.org/10.1016/j.joule.2020.12.025.

[14] J. Gao, N. Shi, Y. Li, B. Jiang, T. Marhaba, W. Zhang, Electrocatalytic upcycling of nitrate wastewater into an ammonia fertilizer via an electrified membrane, Environ. Sci. Technol. 56 (16) (2022) 11602–11613, https://doi.org/10.1021/acs.est.1c08442.

[15] G.N. Schrauzer, T.D. Guth, Photolysis of water and photoreduction of nitrogen on titanium dioxide, J. Am. Chem. Soc. 99 (22) (1977) 7189–7193, https://doi.org/10.1021/ja00464a015.

[16] Y.J. Jang, A.E. Lindberg, M.A. Lumley, K.-S. Choi, Photoelectrochemical nitrogen reduction to ammonia on cupric and cuprous oxide photocathodes, ACS Energy Lett. 5 (6) (2020) 1834–1839, https://doi.org/10.1021/acsenergylett.0c00711.

[17] Y. Bai, H. Bai, K. Qu, F. Wang, P. Guan, D. Xu, W. Fan, W. Shi, In-situ approach to fabricate BiOI photocathode with oxygen vacancies: understanding the N_2 reduced behavior in photoelectrochemical system, Chem. Eng. J. 362 (2019) 349–356, https://doi.org/10.1016/j.cej.2019.01.051.

[18] D. Liu, J. Wang, S. Bian, Q. Liu, Y. Gao, X. Wang, P.K. Chu, X.-F. Yu, Photoelectrochemical synthesis of ammonia with black phosphorus, Adv. Funct. Mater. 30 (24) (2020) 2002731, https://doi.org/10.1002/adfm.202002731.

[19] K. Peramaiah, V. Ramalingam, H.-C. Fu, M.M. Alsabban, R. Ahmad, L. Cavallo, V. Tung, K.-W. Huang, J.-H. He, Optically and electrocatalytically decoupled si photocathodes with a porous carbon nitride catalyst for nitrogen reduction with over 61.8 % faradaic efficiency, Adv. Mater. 33 (18) (2021) 2100812, https://doi.org/10.1002/adma.202100812.

[20] J. Zheng, Y. Lyu, M. Qiao, R. Wang, Y. Zhou, H. Li, C. Chen, Y. Li, H. Zhou, S. P. Jiang, S. Wang, Photoelectrochemical synthesis of ammonia on the aerophilic-hydrophilic heterostructure with 37.8 % efficiency, Chem 5 (3) (2019) 617–633, https://doi.org/10.1016/j.chempr.2018.12.003.

[21] H. Huang, D. Periyanagounder, C. Chen, Z. Li, Q. Lei, Y. Han, K.-W. Huang, J.-H. He, Artificial leaf for solar-driven ammonia conversion at milligram-scale using triple junction III-V photoelectrode, Adv. Sci. 10 (14) (2023) 2205808, https://doi.org/10.1002/advs.202205808.

[22] H.E. Kim, J. Kim, E.C. Ra, H. Zhang, Y.J. Jang, J.S. Lee, Photoelectrochemical nitrate reduction to ammonia on ordered silicon nanowire array photocathodes, Angew. Chem. Int. Ed. 61 (25) (2022) e202204117, https://doi.org/10.1002/anie.202204117.

[23] S. Zhou, K. Sun, C.Y. Toe, J. Yin, J. Huang, Y. Zeng, D. Zhang, W. Chen, O. F. Mohammed, X. Hao, R. Amal, Engineering a Kesterite-based photocathode for photoelectrochemical ammonia synthesis from NO_x reduction, Adv. Mater. 34 (29) (2022) 2201670, https://doi.org/10.1002/adma.202201670.

[24] E. Murphy, Y. Liu, I. Matanovic, S. Guo, P. Tieu, Y. Huang, A. Ly, S. Das, I. Zenyuk, X. Pan, E. Spoerke, P. Atanassov, Highly durable and selective Fe- and Mo-based atomically dispersed electrocatalysts for nitrate reduction to ammonia via distinct and synergized NO_2^- pathways, ACS Catal. 12 (11) (2022) 6651–6662, https://doi.org/10.1021/acscatal.2c01367.

[25] X. Li, W. Fan, Y. Bai, Y. Liu, F. Wang, H. Bai, W. Shi, Photoelectrochemical reduction of nitrate to ammonia over CuPc/CeO_2 heterostructure: understanding the synergistic effect between oxygen vacancies and Ce sites, Chem. Eng. J. 433 (2022) 133225, https://doi.org/10.1016/j.cej.2021.133225.

[26] Y. Xu, K. Ren, T. Ren, M. Wang, Z. Wang, X. Li, L. Wang, H. Wang, Ultralow-content Pd in-situ incorporation mediated hierarchical defects in corner-etched Cu_2O octahedra for enhanced electrocatalytic nitrate reduction to ammonia, Appl. Catal., B 306 (2022) 121094, https://doi.org/10.1016/j.apcatb.2022.121094.

[27] F. Lei, W. Xu, J. Yu, K. Li, J. Xie, P. Hao, G. Cui, B. Tang, Electrochemical synthesis of ammonia by nitrate reduction on indium incorporated in sulfur doped graphene, Chem. Eng. J. 426 (2021) 131317, https://doi.org/10.1016/j.cej.2021.131317.

[28] Y. Li, S. Xiao, X. Li, C. Chang, M. Xie, J. Xu, Z. Yang, A robust metal-free electrocatalyst for nitrate reduction reaction to synthesize ammonia, Mater. Today Phys. 19 (2021) 100431, https://doi.org/10.1016/j.mtphys.2021.100431.

[29] D. He, H. Ooka, Y. Li, Y. Kim, A. Yamaguchi, K. Adachi, D. Hashizume, N. Yoshida, S. Toyoda, S.H. Kim, R. Nakamura, Regulation of the electrocatalytic nitrogen cycle based on sequential proton–electron transfer, Nat. Catal. 5 (9) (2022) 798–806, https://doi.org/10.1038/s41929-022-00833-z.

[30] B. Min, Q. Gao, Z. Yan, X. Han, K. Hosmer, A. Campbell, H. Zhu, Powering the remediation of the nitrogen cycle: progress and perspectives of electrochemical nitrate reduction, Ind. Eng. Chem. Res. 60 (41) (2021) 14635–14650, https://doi.org/10.1021/acs.iecr.1c03072.

[31] Y.F. Tay, H. Kaneko, S.Y. Chiam, S. Lie, Q. Zheng, B. Wu, S.S. Hadke, Z. Su, P. S. Bassi, D. Bishop, Solution-processed Cd-substituted CZTS photocathode for efficient solar hydrogen evolution from neutral water, Joule 2 (3) (2018) 537–548.

[32] D. Huang, K. Wang, L. Li, K. Feng, N. An, S. Ikeda, Y. Kuang, Y. Ng, F. Jiang, 3.17 % efficient Cu_2ZnSnS_4–$BiVO_4$ integrated tandem cell for standalone overall solar water splitting, Energy Environ. Sci. 14 (3) (2021) 1480–1489, https://doi.org/10.1039/d0ee03892j.

[33] A. Wang, J. Huang, J. Cong, X. Yuan, M. He, J. Li, C. Yan, X. Cui, N. Song, S. Zhou, M.A. Green, K. Sun, X. Hao, Cd-Free pure sulfide kesterite Cu_2ZnSnS_4 solar cell with over 800 mV open-circuit voltage enabled by phase evolution intervention, Adv. Mater. n/a (n/a) (2023) 2307733, https://doi.org/10.1002/adma.202307733.

[34] M.A. Gaikwad, U.P. Suryawanshi, U.V. Ghorpade, J.S. Jang, M.P. Suryawanshi, J. H. Kim, Emerging surface, bulk, and interface engineering strategies on $BiVO_4$ for photoelectrochemical water splitting, Small 18 (10) (2022) 2105084, https://doi.org/10.1002/smll.202105084.

[35] X. Chang, T. Wang, P. Yang, G. Zhang, J. Gong, The development of cocatalysts for photoelectrochemical CO_2 reduction, Adv. Mater. 31 (31) (2019) 1804710.

[36] D. Li, K. Yang, J. Lian, J. Yan, S. Liu, Powering the world with solar fuels from photoelectrochemical CO_2 reduction: basic principles and recent advances, Adv. Energy Mater. 12 (31) (2022) 2201070, https://doi.org/10.1002/aenm.202201070.

[37] Y. Wang, C. Wang, M. Li, Y. Yu, B. Zhang, Nitrate electroreduction: mechanism insight, in situ characterization, performance evaluation, and challenges, Chem. Soc. Rev. 50 (12) (2021) 6720–6733, https://doi.org/10.1039/D1CS00116G.

[38] X. Zhang, Y. Wang, C. Liu, Y. Yu, S. Lu, B. Zhang, Recent advances in non-noble metal electrocatalysts for nitrate reduction, Chem. Eng. J. 403 (2021) 126269, https://doi.org/10.1016/j.cej.2020.126269.

[39] Y. Bi, H. Hu, G. Lu, Highly ordered rectangular silver nanowire monolayers: water-assisted synthesis and galvanic replacement reaction with $HAuCl_4$, Chem. Commun. 46 (4) (2010) 598–600, https://doi.org/10.1039/B911777F.

[40] H. Du, T. Wan, B. Qu, F. Cao, Q. Lin, N. Chen, X. Lin, D. Chu, Engineering silver nanowire networks: from transparent electrodes to resistive switching devices, ACS Appl. Mater. Interfaces 9 (24) (2017) 20762–20770, https://doi.org/10.1021/acsami.7b04839.

[41] W. Septina, Gunawan, S. Ikeda, T. Harada, M. Higashi, R. Abe, M. Matsumura, Photosplitting of water from wide-gap Cu(In,Ga)S_2 thin films modified with a CdS Layer and Pt nanoparticles for a high-onset-potential photocathode, J. Phys. Chem. C 119 (16) (2015) 8576–8583, https://doi.org/10.1021/acs.jpcc.5b02068.

[42] Z. Mei, Y. Chen, S. Tong, Y. Li, J. Liu, L. Sun, W. Zhong, X. Dong, Y. Ji, Y. Lin, H. Chen, F. Pan, High-performance Si photocathode enabled by spatial decoupling multifunctional layers for water splitting, Adv. Funct. Mater. 32 (2) (2022) 2107164, https://doi.org/10.1002/adfm.202107164.

[43] H.Y. Chung, C.Y. Toe, W. Chen, X. Wen, R.J. Wong, R. Amal, F.F. Abdi, Y.H. Ng, Manipulating the fate of charge carriers with tungsten concentration: enhancing photoelectrochemical water oxidation of Bi_2WO_6, Small 17 (35) (2021) 2102023, https://doi.org/10.1002/smll.202102023.

[44] F.B. Li, X.Z. Li, M.F. Hou, Photocatalytic degradation of 2-mercaptobenzothiazole in aqueous La^{3+}–TiO_2 suspension for odor control, Appl. Catal., B 48 (3) (2004) 185–194, https://doi.org/10.1016/j.apcatb.2003.10.003.

[45] M. Li, P. Wang, Z. Ji, Z. Zhou, Y. Xia, Y. Li, S. Zhan, Efficient photocatalytic oxygen activation by oxygen-vacancy-rich CeO_2-based heterojunctions: synergistic effect of photoexcited electrons transfer and oxygen chemisorption, Appl. Catal., B 289 (2021) 120020, https://doi.org/10.1016/j.apcatb.2021.120020.

[46] C. Su, L. Liu, M. Zhang, Y. Zhang, C. Shao, Fabrication of Ag/TiO_2 nanoheterostructures with visible light photocatalytic function via a solvothermal approach, CrystEngComm 14 (11) (2012) 3989–3999, https://doi.org/10.1039/C2CE25161B.

[47] F. Su, T. Wang, R. Lv, J. Zhang, P. Zhang, J. Lu, J. Gong, Dendritic Au/TiO_2 nanorod arrays for visible-light driven photoelectrochemical water splitting, Nanoscale 5 (19) (2013) 9001–9009, https://doi.org/10.1039/C3NR02766J.

[48] H. Zhang, Y. Zhao, S. Chen, B. Yu, J. Xu, H. Xu, L. Hao, Z. Liu, Ti^{3+} self-doped TiO_x@anatase core–shell structure with enhanced visible light photocatalytic

activity, J. Mater. Chem. A 1 (20) (2013) 6138–6144, https://doi.org/10.1039/C3TA10413C.
[49] A. Ziarati, A. Badiei, R. Luque, Black hollow TiO_2 nanocubes: advanced nanoarchitectures for efficient visible light photocatalytic applications, Appl. Catal., B 238 (2018) 177–183, https://doi.org/10.1016/j.apcatb.2018.07.020.
[50] W. Meng, Z. Dang, D. Li, L. Jiang, D. Fang, Interface and defect engineered titanium-base oxide heterostructures synchronizing high-rate and ultrastable sodium storage, Adv. Energy Mater. 12 (40) (2022) 2201531, https://doi.org/10.1002/aenm.202201531.
[51] A.G.M. da Silva, C.G. Fernandes, Z.D. Hood, R. Peng, Z. Wu, A.H.B. Dourado, L. S. Parreira, D.C. de Oliveira, P.H.C. Camargo, S.I.C. de Torresi, PdPt-TiO_2 nanowires: correlating composition, electronic effects and O-vacancies with activities towards water splitting and oxygen reduction, Appl. Catal., B 277 (2020) 119177, https://doi.org/10.1016/j.apcatb.2020.119177.
[52] H. Yuan, S.A.A.A. Aljneibi, J. Yuan, Y. Wang, H. Liu, J. Fang, C. Tang, X. Yan, H. Cai, Y. Gu, S.J. Pennycook, J. Tao, D. Zhao, ZnO Nanosheets abundant in oxygen vacancies derived from metal-organic frameworks for ppb-level gas sensing, Adv. Mater. 31 (11) (2019) 1807161, https://doi.org/10.1002/adma.201807161.
[53] C. Guo, X. Liu, L. Gao, X. Ma, M. Zhao, J. Zhou, X. Kuang, W. Deng, X. Sun, Q. Wei, Oxygen defect engineering in cobalt iron oxide nanosheets for promoted overall water splitting, J. Mater. Chem. A 7 (38) (2019) 21704–21710, https://doi.org/10.1039/C9TA06537G.
[54] Q. Liu, Q. Wang, J. Wang, Z. Li, J. Liu, X. Sun, J. Li, Y. Lei, L. Dai, P. Wang, $TpyCo^{2+}$-Based coordination polymers by water-induced gelling trigged efficient oxygen evolution reaction, Adv. Funct. Mater. 30 (38) (2020) 2000593, https://doi.org/10.1002/adfm.202000593.
[55] J. Yang, S. Ren, Y. zhou, Z. Su, L. Yao, J. Cao, L. Jiang, G. Hu, M. Kong, J. Yang, Q. Liu, In situ IR comparative study on N_2O formation pathways over different valence states manganese oxides catalysts during NH_3–SCR of NO, Chem. Eng. J. 397 (2020) 125446, https://doi.org/10.1016/j.cej.2020.125446.
[56] M. Chen, Q. Jin, X. Tao, Y. Pan, S. Gu, Y. Shen, Novel $WZrO_x/TiO_2$ catalyst for selective catalytic reduction of NO by NH3 at high temperature, Catal. Today 358 (2020) 254–262, https://doi.org/10.1016/j.cattod.2019.06.045.
[57] F. Zasada, P.V.B. Pinho, W. Piskorz, C. Hudy, J. Janas, J. Gryboś, K. Góra-Marek, Z. Sojka, Adsorption of NO_2 and NO_3 on Cobalt spinel nanocubes and interfacial dynamics of the resultant NO_x adspecies (x = 1, 2, and 3): DFT, atomistic thermodynamic, IR, and isotopic exchange study, J. Phys. Chem. C 124 (36) (2020) 19681–19697, https://doi.org/10.1021/acs.jpcc.0c06195.
[58] H. Liu, X. Lang, C. Zhu, J. Timoshenko, M. Rüscher, L. Bai, N. Guijarro, H. Yin, Y. Peng, J. Li, Z. Liu, W. Wang, B.R. Cuenya, J. Luo, Efficient electrochemical nitrate reduction to ammonia with copper-supported rhodium cluster and single-atom catalysts, Angew. Chem. Int. Ed. 61 (23) (2022) e202202556, https://doi.org/10.1002/anie.202202556.
[59] S. Liu, M. Wang, H. Ji, L. Zhang, J. Ni, N. Li, T. Qian, C. Yan, J. Lu, Solvent-in-gas system for promoted photocatalytic ammonia synthesis on porous framework materials, Adv. Mater. 35 (14) (2023) 2211730, https://doi.org/10.1002/adma.202211730.
[60] Z.-Y. Wu, M. Karamad, X. Yong, Q. Huang, D.A. Cullen, P. Zhu, C. Xia, Q. Xiao, M. Shakouri, F.-Y. Chen, J.Y. Kim, Y. Xia, K. Heck, Y. Hu, M.S. Wong, Q. Li, I. Gates, S. Siahrostami, H. Wang, Electrochemical ammonia synthesis via nitrate reduction on Fe single atom catalyst, Nat. Commun. 12 (1) (2021) 2870, https://doi.org/10.1038/s41467-021-23115-x.
[61] H. Xu, Y. Ma, J. Chen, W.-x Zhang, J. Yang, Electrocatalytic reduction of nitrate – a step towards a sustainable nitrogen cycle, Chem. Soc. Rev. 51 (7) (2022) 2710–2758, https://doi.org/10.1039/D1CS00857A.
[62] B.A. Pinaud, J.D. Benck, L.C. Seitz, A.J. Forman, Z. Chen, T.G. Deutsch, B.D. James, K.N. Baum, G.N. Baum, S. Ardo, H. Wang, E. Miller, T.F. Jaramillo, Technical and economic feasibility of centralized facilities for solar hydrogen production via photocatalysis and photoelectrochemistry, Energy Environ. Sci. 6 (7) (2013) 1983–2002, https://doi.org/10.1039/C3EE40831K.
[63] A. Rothschild, H. Dotan, Beating the efficiency of photovoltaics-powered electrolysis with tandem cell photoelectrolysis, ACS Energy Lett. 2 (1) (2017) 45–51, https://doi.org/10.1021/acsenergylett.6b00610.